nature physics

Article

https://doi.org/10.1038/s41567-024-02761-0

Constraints on the location of the liquid–liquid critical point in water

Received: 17 May 2024

Accepted: 10 December 2024

Published online: 03 February 2025

Check for updates

F. Sciortino [1], Y. Zhai [2,3,7], S. L. Bore [2,8] & F. Paesani [2,4,5,6]

The fascinating hypothesis that supercooled water may segregate into two distinct liquid phases, each with unique structures and densities, was first posited in 1992. This idea, initially based on numerical analyses with the ST2 water-like empirical potential, challenged the conventional understanding of water's phase behaviour at the time and has since intrigued the scientific community. Over the past three decades, advancements in computational modelling—particularly through the advent of data-driven many-body potentials rigorously derived from first principles and augmented by the efficiency of neural networks—have greatly enhanced the accuracy of molecular simulations, enabling the exploration of the phase behaviour of water with unprecedented realism. Our study leverages these computational advances to probe the elusive liquid–liquid transition in supercooled water. Microsecond-long simulations with chemical accuracy, conducted over several years, provide compelling evidence that water indeed exists in two discernibly distinct liquid states at low temperature and high pressure. By pinpointing a realistic estimate for the location of the liquid–liquid critical point at ~198 K and ~1,250 atm, our study not only advances the current understanding of water's anomalous behaviour but also establishes a basis for experimental validation. Importantly, our simulations indicate that the liquid–liquid critical point falls within temperature and pressure ranges that could potentially be experimentally probed in water nanodroplets, opening up the possibility for direct measurements.

Water, life's matrix[1], also happens to be one of the most peculiar liquids on Earth[2]. Its unusual temperature- and pressure-dependent thermodynamic response properties have puzzled and, at the same time, fascinated scientists for a long time[3]. Numerous noteworthy experiments have been conducted over the past decade[4–10], demonstrating that what was once considered an uncharted territory in the phase diagram of water (due to fast crystallization) can indeed be explored in the laboratory. Particularly relevant have been the experiments demonstrating the existence of compressibility maxima on isobaric cooling both at positive[6] and negative[5] pressures, and the demonstration that a laser-heated high-density glass sample undergoes a crossover from a high-density liquid (HDL) structure to a low-density liquid (LDL) one in the submicrosecond time window[7].

Over the past decade, it has become increasingly apparent that further experimental progress strongly depends on the precise estimate of the liquid–liquid critical parameters, that is, critical temperature (T_c) and pressure (P_c). In this context, computational models play a crucial role in directing experimental studies towards the specific

[1]Dipartimento di Fisica, Sapienza Università di Roma, Rome, Italy. [2]Department of Chemistry and Biochemistry, University of California San Diego, La Jolla, CA, USA. [3]Department of Computer Science and Engineering, University of California San Diego, La Jolla, CA, USA. [4]Materials Science and Engineering, University of California San Diego, La Jolla, CA, USA. [5]Halıcıoğlu Data Science Institute, University of California San Diego, La Jolla, CA, USA. [6]San Diego Supercomputer Center, University of California San Diego, La Jolla, CA, USA. [7]Present address: Amazon.com, Inc., Seattle, WA, USA. [8]Present address: Hylleraas Centre for Quantum Molecular Sciences and Department of Chemistry, University of Oslo, Oslo, Norway. e-mail: fpaesani@ucsd.edu

temperature and pressure ranges in which the liquid–liquid transition of water is likely to be observed. Despite their success in reproducing some properties of water[11], empirical pairwise-additive models fall short at providing a reliable representation of water across all its phases, requiring ad hoc temperature and/or pressure shifts to be effectively compared with experimental measurements[12,13]. Similarly, ab initio models derived from density functional theory (DFT)[14] have been widely used in simulations of water, but—in practice—suffer from both functional- and density-driven errors[15–17] that limit their accuracy and transferability across phases[18–20]. These limitations often lead to non-physical predictions of the critical parameters, further complicating the reliability of DFT-derived ab initio models in accurately representing the phase behaviour of water at the molecular level[21,22]. Models developed using the adaptive force matching method, such as the water model from adaptive force matching for ice and liquid (WAIL)[23] and its revised version rWAIL[24], also predict a liquid–liquid transition. The WAIL model, predicts a fairly low critical pressure due to the difficulties in handling the long-range corrections to pressure. In rWAIL, where such a limitation has been corrected, the estimated critical point location shifts to ~200 K and ~900 atm. As shown in Supplementary Fig. 2, neither WAIL nor rWAIL (similar to other water models) reproduces the experimental isothermal compressibility measured at ambient pressure.

As a consequence of the limited accuracy of existing empirical and ab initio water models, a wide range in estimates for the critical pressure (P_c from ~36 to ~270 MPa) and temperature (T_c from ~150 to ~250 K) has been reported by previous theoretical and computational studies[12,22,23,25–27]. Besides reflecting the high dependency of critical parameters on the specific water model used in the simulations, the uncertainty associated with the location of a possible liquid–liquid critical point in water points to a major gap in our fundamental understanding of water's phase behaviour. This variability poses a substantial challenge for both theoretical predictions and practical applications, necessitating realistic models for a unified and physically accurate representation of water's critical phenomena[12,23,25,28–34].

Progress in correlated electronic structure methods[35,36] has recently enabled routine calculations of interaction energies for small water clusters at the coupled cluster level of theory, including single, double and perturbative triple excitation, that is, CCSD(T), the current gold standard of chemical accuracy for molecular interactions[37,38]. These developments have led to the introduction of a new class of data-driven models of water, derived entirely from first principles. These models rigorously decompose the interaction energy of a water system, consisting of N molecules, into individual n-body contributions ($n = 1, 2...N$), which can be efficiently calculated at the CCSD(T) level of theory[39–41]. Among these first-principles data-driven many-body models, MB-pol[42–44] has been shown to provide a realistic representation of water across all phases at pressures below ~1 GPa (refs. 45,46), where ice rules violation and partial molecular dissociation are not effective. MB-pol achieves this high level of realism by integrating machine-learned representations of short-range n-body quantum-mechanical effects, such as Pauli repulsion and charge transfer, with mean-field-like representations of many-body electrostatic interactions. This theoretical/computational framework ensures that MB-pol accurately reproduces the CCSD(T) reference data for diverse water systems[41]. MB-pol consistently predicts thermodynamic, dynamical and spectroscopic properties of gas-phase water clusters, liquid water and ice, in agreement with the corresponding experimental values[47,48]. MB-pol accurately predicts the stability regions of all ice polymorphs below 1 GPa, closely reproducing the experimental phase diagram of water within this pressure range (a brief overview of the MB-pol potential is provided in Supplementary Section 1).

Building on the accuracy and predictive power of MB-pol, a deep neural network model (DNN@MB-pol)[46] has recently been developed within the DeePMD framework[49–51] from an extensive training set of MB-pol configurations for both liquid water and ice, spanning a wide range of temperatures and pressures. Although DNN@MB-pol is not an exact surrogate model for MB-pol over the entire phase diagram of water, it closely reproduces the properties of liquid water at 1 atm as predicted by MB-pol, from the boiling point down to deeply supercooled temperatures[46]. Among the DeePMD-based potentials trained on the MB-pol data reported in the literature[52,53], DNN@MB-pol has been shown to provide the most robust representation of MB-pol[54] (a brief overview of the DNN@MB-pol potential is provided in Supplementary Section 2). The primary advantage of DNN@MB-pol lies in its computational efficiency. By leveraging the high parallelization capabilities of deep neural networks on graphical processing units, DNN@MB-pol enables molecular dynamics (MD) simulations of liquid water at a substantially reduced computational cost compared with the parent MB-pol potential. Despite its efficiency, microsecond-long MD simulations of supercooled water with DNN@MB-pol are still computationally fairly demanding, requiring several months of graphical processing unit time for each investigated state point.

In this study, we harness the realism and computational efficiency of the DNN@MB-pol potential to explore the phase behaviour of supercooled water across a broad range of temperatures and pressures through microsecond-long MD simulations, effectively achieving CCSD(T) accuracy. This level of performance remains prohibitively expensive and currently unattainable by any other means, not just for water but for any molecular species. Our analyses support the existence of a liquid–liquid critical point, although at pressures substantially lower than those estimated using empirical and DFT models. Our findings not only provide the first realistic molecular picture of supercooled water but also open new avenues for experimental validation and further exploration of water's phase behaviour at low temperature and high pressure.

Mass density fluctuations in supercooled water

Figure 1a shows the temperature and pressure dependence of the mass density of liquid water, ρ, calculated from DNN@MB-pol simulations carried out in the isobaric–isothermal ensemble (NPT = constant number of molecules N, pressure P and temperature T) at 280 different state points across 20 temperatures between 188 K and 368 K, and 14 pressures ranging from 1 atm to 1,300 atm. The variation in isothermal compressibility across the same temperature and pressure ranges is shown in Supplementary Fig. 7. It is important to note that none of the simulations were found to contain any crystalline aggregate (as detected by the CHILL+ algorithm[55] or bond orientation order parameters[56]) at the end of the MD trajectories. All curves exhibit a distinct mass density maximum, characteristic of water's anomalous expansion on cooling. As the pressure increases, this maximum becomes less pronounced and shifts to lower temperatures, with the crossover from high density to low density on cooling becoming increasingly sharper, up to approximately $P = 1{,}000$ atm. Although the variation in water's mass density predicted by DNN@MB-pol as a function of temperature and pressure aligns qualitatively with previous simulation studies, the jump in mass density at low T hints at the existence of a metastable liquid–liquid critical point in supercooled water at pressures that are substantially lower than those predicted by empirical and DFT water models.

The existence of a metastable liquid–liquid critical point is reinforced by the analysis of the time dependence of mass density fluctuations predicted by DNN@MB-pol for supercooled water at a given state point. To this end, Fig. 1b shows the variation in water's mass density along NPT trajectories carried out at 188 K under three different pressures (800 atm, 1,000 atm and 1,200 atm), providing direct evidence for the ability of supercooled water to access two distinct states. In particular, the DNN@MB-pol trajectory at 1,000 atm (and similarly for adjacent pressure values) exhibits large mass density fluctuations that occur on a microsecond timescale and connect two

https://doi.org/10.1038/s41567-024-02761-0

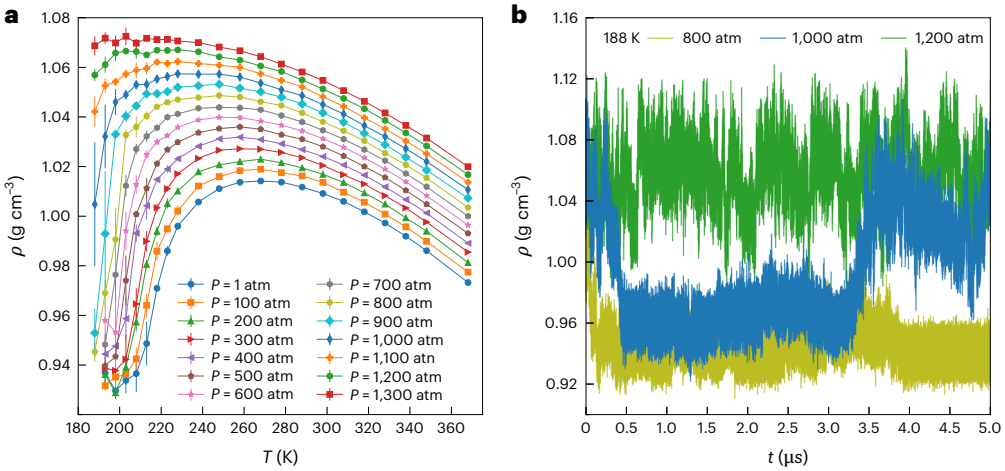

Fig. 1 | Temperature and pressure dependence of the mass density of liquid water. a, Mass density of water, ρ, as predicted by DNN@MB-pol simulations carried out in the *NPT* ensemble as a function of temperature and pressure. Each *NPT* trajectory was divided into four blocks of equal length, with ρ calculated for each block and then averaged. The error bars represent the 95% confidence intervals, derived from the standard error of the mean across the blocks. **b**, Time dependence of ρ at 188 K calculated from microsecond-long *NPT* simulations carried out with DNN@MB-pol at 800 atm, 1,000 atm and 1,200 atm.

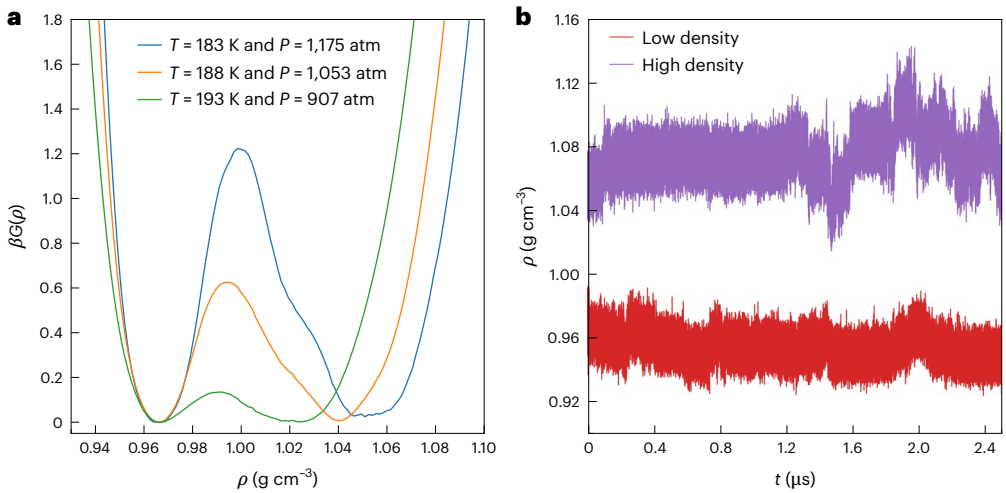

Fig. 2 | Free-energy landscape of supercooled water. a, Gibbs free-energy profiles as a function of mass density ρ for three thermodynamic state points. **b**, Variation in ρ at 178 K and 1,270 atm calculated along two independent microsecond-long trajectories started from low-density (red) and high-density (violet) configurations.

distinct liquid states, an LDL state and an HDL state. Figure 1b clearly shows that the LDL and HDL states correspond to the equilibrium states of supercooled water at 188 K and low (800 atm) and high (1,200 atm) pressures, respectively.

Free-energy landscape of supercooled water

To maximize the information contained in the comprehensive set of *NPT* simulations with DNN@MB-pol, the most accurate representation of the density of states with energy E and volume V, denoted as $\Omega(V, E)$, was calculated via the weighted histogram analysis procedures[57], extended to the *NPT* ensemble[58] (a brief overview of the weighted histogram method is provided in Supplementary Section 3). From $\Omega(V, E)$, it is possible to derive all the thermodynamic properties of the system. In particular, the density of states facilitates the calculation of free-energy profiles at and below the temperatures directly explored in the *NPT* simulations. Figure 2a displays the Gibbs free-energy profiles, βG, as a function of the mass density for three temperatures in the neighbourhood of T_c. For each temperature, βG is plotted at the pressure at which the depths of the two minima are equivalent. For all the three state points considered in Fig. 2a, the corresponding free-energy profiles exhibit a well-defined double-well shape, with a barrier height that increases on cooling—a hallmark of the emergence of a first-order phase transition between two disordered phases. The local curvature of the two wells is a measure of the isothermal compressibility of the two liquids. The LDL has a narrower basin than the HDL, indicating smaller mass density fluctuations in the LDL. This difference in isothermal compressibility is also consistent with previous estimates based on the equation of state[12]. At $T = 188$ K, the barrier height is approximately $0.60 k_B T$ (k_B is Boltzmann's constant). Within the Ising universality class, a barrier height of $0.77 k_B T$ is indicative of the critical temperature in a finite-sized system when the mass density serves as the order parameter. Despite extensive computational efforts, the data from the present microsecond-long simulations with the DNN@MB-pol potential are still not sufficient for a precise comparison with the Ising universality class predictions based on mixed energy and mass density fluctuations. As a result, the criterion of barrier height emerges as the most reliable method to estimate the critical point as predicted by the DNN@MB-pol potential. This yields a critical temperature $T_c = 188 \pm 5$ K and

https://doi.org/10.1038/s41567-024-02761-0

a critical pressure P_c = 1,050 ± 50 atm. In particular, approximately 5 K below this temperature, the barrier height rises to $1.2k_BT$, consistent with recent estimates from other water models at similar relative temperatures $(T - T_c)/T_c$ (refs. 22,33,59). As discussed in the Methods, our analyses pertain to a system of N = 256 water molecules. Although finite-size effects cannot be entirely ruled out, simulations conducted with models based on effective pairwise-additive interactions, where such analyses have been performed, suggest a weak dependence of the critical parameters T_c and P_c on the system size[27,29].

As an additional investigation into the existence of a first-order transition between two distinct liquid phases, Fig. 2b depicts the time evolution of the densities of the LDL and HDL phases at T = 178 K, at a pressure approximately lying on the LDL–HDL coexistence line as determined by the density of states. This analysis unequivocally demonstrates that at this state point, the LDL and HDL phases remain distinctly separated within their respective free-energy basins for several microseconds, exhibiting markedly different densities throughout the course of the corresponding *NPT* simulations. The persistent separation and distinct densities of the LDL and HDL phases under these conditions provides further evidence for the presence of a first-order transition between the two liquid phases at slightly higher temperature and lower pressure relative to this state point. To characterize the structural changes associated with LDL and HDL configurations, Supplementary Fig. 8 shows the oxygen–oxygen radial distribution functions and corresponding structure factors calculated from the same *NPT* simulations (Fig. 2b).

Phase diagram of supercooled water

Figure 3 summarizes the phase behaviour of supercooled water as predicted by the DNN@MB-pol potential. The liquid–liquid coexistence curve departs from the critical point, with a negative slope of −21.4 bar K^{-1}. By applying the Clausius–Clapeyron equation, this negative slope corresponds to an entropy change between the two liquid phases of ~3.5 J mol^{-1} K^{-1} at T = 183 K, confirming that the HDL phase is more 'disordered' despite being more dense. Two spinodal lines emerge from the critical point for $T \leq T_c$, indicating the limit of metastability of each of the two liquid phases. At pressures lower than the HDL spinodal pressure, any HDL sample will immediately decompose into regions of low and high mass density via a spinodal mechanism, consistent with experimental results probing the so-called no man's land in the phase diagram of water on the submicrosecond timescale[7]. For $T \geq T_c$, the Widom line (corresponding to the locus of maximum fluctuations along isobars) departs from the critical point and reaches the ambient pressure at 217 K. The value predicted by the DNN@MB-pol potential is in excellent agreement with the experimental estimate of 225 K (ref. 6). This behaviour is evident in the temperature dependence of the isothermal compressibility calculated with the DNN@MB-pol potential in the pressure range of 1–1,300 atm (Supplementary Fig. 7). To further characterize the molecular configurations of supercooled water near the critical point, Supplementary Fig. 9 shows the two-dimensional density distributions representing the probabilities of observing configurations with specific energy and mass density values calculated at two different state points near the critical point. Both two-dimensional probability densities clearly indicate the presence of two distinct basins.

The phase diagram in Fig. 3 also shows the isobaric temperature of the maximum mass density line. At ambient pressure, the temperature of the maximum mass density predicted by the DNN@MB-pol potential is ~267 K, approximately 10 K below the experimental value. A same shift of ~10 K between the DNN@MB-pol predictions and experimental data for the isobaric temperature of maximum densities is observed across the entire pressure range shown in Fig. 3. Finally, the liquid–ice I_h coexistence line predicted by the DNN@MB-pol potential is also consistently shifted by ~10 K compared with the experimental line, over the entire pressure range. These comparisons indicate that DNN@MB-pol correctly predicts the shape of the phase diagram of

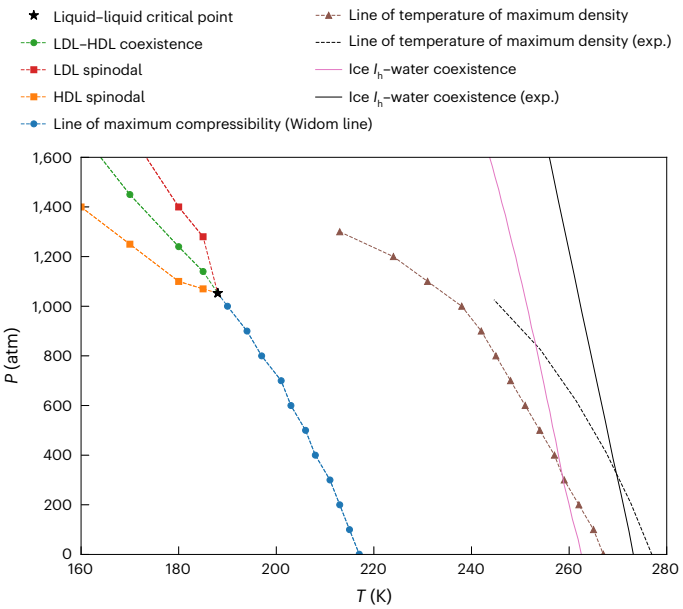

Fig. 3 | Phase diagram of supercooled water. All symbols refer to data obtained from *NPT* simulations carried out with the DNN@MB-pol potential presented in this study. Also shown is the line of temperature of maximum mass density derived from the experimental data (dashed black line) as well as the DNN@MB-pol (solid pink line) and experimental (solid black line) ice I_h–water coexistence lines[46].

supercooled water within the temperature and pressure ranges shown in Fig. 3, although effectively shifted to lower temperatures by ~10 K. It should be noted that the liquid–ice I_h coexistence line predicted by DNN@MB-pol closely follows the corresponding line predicted by the parent MB-pol potential[46], confirming that the former represents a reliable—although not exact—surrogate model for the latter.

Conclusion

The MB-pol potential, which was rigorously derived from first principles using state-of-the-art CCSD(T) electronic structure data[42–44], stands out for its accuracy in reproducing the phase diagram of water across gas, liquid and various crystalline phases[45–47]. Recent progress in machine learning algorithms[49–51] has enabled the development of the DNN@MB-pol potential, a computationally efficient deep neural network surrogate for the MB-pol potential. Remarkably, the only difference between the predictions of the DNN@MB-pol potential and actual water properties is a subtle shift of about 10 K and 200 atm towards lower temperatures and pressures, respectively. It, thus, follows that the identification of a liquid–liquid critical point within the DNN@MB-pol phase diagram of supercooled water—achieved through microsecond-long MD simulations that spanned several years of graphical processing unit computational effort—provides strong support for the thermodynamic hypothesis proposed earlier[12]. Besides providing realistic estimates for the critical temperature and pressure, currently elusive to experimental measurements, our study also reveals that the values of the critical parameters (T_c and P_c) notably differ from those predicted by previous studies using empirical and DFT models of water. Considering the ~10 K and ~200 atm shifts in the DNN@MB-pol phase diagram relative to the experimental phase diagram (Supplementary Fig. 5), the critical parameters predicted for DNN@MB-pol water suggests an actual critical point in liquid water at $T_c \approx 198 \pm 5$ K and $P_c \approx 1{,}250 \pm 50$ atm. The critical pressure is substantially lower than predictions from DFT models of water[29], but consistent with recent polynomial extrapolations of the equation of state derived from experimental data[60]. This relatively low critical pressure not only pinpoints the pressure range

crucial for future experiments on critical fluctuations but also paves the way for directly probing the liquid–liquid critical point in nanodroplets composed of thousands of molecules, where such pressures are potentially attainable through leveraging Laplace pressure[61]. Our results, thus, set a clear direction for future measurements and offer a feasible approach to study the critical behaviour of supercooled water in a controlled experimental setting. Our findings further underscore that DNN@MB-pol (and by extension, MB-pol) serves as a highly realistic model of water, capable of accurately simulating its behaviour across diverse environments and thermodynamic conditions. Such transferability is crucial across a broad spectrum of disciplines, from biology and biochemistry to materials science and environmental sciences, where the unique properties of water play a central role in several fundamental processes.

Online content

Any methods, additional references, Nature Portfolio reporting summaries, source data, extended data, supplementary information, acknowledgements, peer review information; details of author contributions and competing interests; and statements of data and code availability are available at https://doi.org/10.1038/s41567-024-02761-0.

References

1. Ball, P. *Life's Matrix: A Biography of Water* (Univ. of California Press, 2001).
2. Eisenberg, D. & Kauzmann, W. *The Structure and Properties of Water* (Clarendon Press, 1969).
3. Speedy, R. & Angell, C. Isothermal compressibility of supercooled water and evidence for a thermodynamic singularity at −45 °C. *J. Chem. Phys.* **65**, 851–858 (1976).
4. Amann-Winkel, K. et al. Water's second glass transition. *Proc. Natl Acad. Sci. USA* **110**, 17720–17725 (2013).
5. Azouzi, M. E. M., Ramboz, C., Lenain, J.-F. & Caupin, F. A coherent picture of water at extreme negative pressure. *Nat. Phys.* **9**, 38–41 (2013).
6. Kim, K. H. et al. Maxima in the thermodynamic response and correlation functions of deeply supercooled water. *Science* **358**, 1589–1593 (2017).
7. Kim, K. H. et al. Experimental observation of the liquid-liquid transition in bulk supercooled water under pressure. *Science* **370**, 978–982 (2020).
8. Kringle, L., Thornley, W. A., Kay, B. D. & Kimmel, G. A. Structural relaxation and crystallization in supercooled water from 170 to 260 K. *Proc. Natl Acad. Sci. USA* **118**, e2022884118 (2021).
9. Mishima, O. *Liquid-Phase Transition in Water* (Springer, 2021).
10. Amann-Winkel, K. et al. Liquid-liquid phase separation in supercooled water from ultrafast heating of low-density amorphous ice. *Nat. Commun.* **14**, 442 (2023).
11. Vega, C. & Abascal, J. L. Simulating water with rigid non-polarizable models: a general perspective. *Phys. Chem. Chem. Phys.* **13**, 19663–19688 (2011).
12. Poole, P. H., Sciortino, F., Essmann, U. & Stanley, H. E. Phase behaviour of metastable water. *Nature* **360**, 324–328 (1992).
13. Espinosa, J. R., Abascal, J. L. F., Sedano, L. F., Sanz, E. & Vega, C. On the possible locus of the liquid–liquid critical point in real water from studies of supercooled water using the TIP4P/Ice model. *J. Chem. Phys.* **158**, 204505 (2023).
14. Gillan, M. J., Alfe, D. & Michaelides, A. Perspective: how good is DFT for water? *J. Chem. Phys.* **144**, 130901 (2016).
15. Vuckovic, S., Song, S., Kozlowski, J., Sim, E. & Burke, K. Density functional analysis: the theory of density-corrected DFT. *J. Chem. Theory Comput.* **15**, 6636–6646 (2019).
16. Song, S., Vuckovic, S., Sim, E. & Burke, K. Density-corrected DFT explained: questions and answers. *J. Chem. Theory Comput.* **18**, 817–827 (2022).
17. Sim, E., Song, S., Vuckovic, S. & Burke, K. Improving results by improving densities: density-corrected density functional theory. *J. Am. Chem. Soc.* **144**, 6625–6639 (2022).
18. Dasgupta, S., Lambros, E., Perdew, J. P. & Paesani, F. Elevating density functional theory to chemical accuracy for water simulations through a density-corrected many-body formalism. *Nat. Commun.* **12**, 6359 (2021).
19. Lambros, E., Hu, J. & Paesani, F. Assessing the accuracy of the SCAN functional for water through a many-body analysis of the adiabatic connection formula. *J. Chem. Theory Comput.* **17**, 3739–3749 (2021).
20. Palos, E. et al. Assessing the interplay between functional-driven and density-driven errors in DFT models of water. *J. Chem. Theory Comput.* **18**, 3410–3426 (2022).
21. Gartner III, T. E. et al. Signatures of a liquid–liquid transition in an ab initio deep neural network model for water. *Proc. Natl Acad. Sci. USA* **117**, 26040–26046 (2020).
22. Gartner III, T. E., Piaggi, P. M., Car, R., Panagiotopoulos, A. Z. & Debenedetti, P. G. Liquid-liquid transition in water from first principles. *Phys. Rev. Lett.* **129**, 255702 (2022).
23. Li, Y., Li, J. & Wang, F. Liquid–liquid transition in supercooled water suggested by microsecond simulations. *Proc. Natl Acad. Sci. USA* **110**, 12209–12212 (2013).
24. Weldon, R. & Wang, F. Water potential from adaptive force matching for ice and liquid with revised dispersion predicts supercooled liquid anomalies in good agreement with two independent experimental fits. *J. Phys. Chem. B* **128**, 3398–3407 (2024).
25. Ni, Y. & Skinner, J. Evidence for a liquid-liquid critical point in supercooled water within the E3B3 model and a possible interpretation of the kink in the homogeneous nucleation line. *J. Chem. Phys.* **144**, 214501 (2016).
26. Debenedetti, P. G., Sciortino, F. & Zerze, G. H. Second critical point in two realistic models of water. *Science* **369**, 289–292 (2020).
27. Eltareb, A., Lopez, G. E. & Giovambattista, N. Evidence of a liquid–liquid phase transition in H_2O and D_2O from path-integral molecular dynamics simulations. *Sci. Rep.* **12**, 6004 (2022).
28. Palmer, J. C. et al. Metastable liquid–liquid transition in a molecular model of water. *Nature* **510**, 385–388 (2014).
29. Palmer, J. C., Poole, P. H., Sciortino, F. & Debenedetti, P. G. Advances in computational studies of the liquid–liquid transition in water and water-like models. *Chem. Rev.* **118**, 9129–9151 (2018).
30. Sciortino, F., Saika-Voivod, I. & Poole, P. H. Study of the ST2 model of water close to the liquid–liquid critical point. *Phys. Chem. Chem. Phys.* **13**, 19759–19764 (2011).
31. Pathak, H. et al. The structural validity of various thermodynamical models of supercooled water. *J. Chem. Phys.* **145**, 134507 (2016).
32. Weis, J., Sciortino, F., Panagiotopoulos, A. Z. & Debenedetti, P. G. Liquid–liquid criticality in the WAIL water model. *J. Chem. Phys.* **157**, 024502 (2022).
33. Dhabal, D., Kumar, R. & Molinero, V. Liquid-liquid transition in a machine-learned coarse grained water model. *Proc. Natl Acad. Sci. USA* **121**, e2322853121 (2024).
34. Neophytou, A. & Sciortino, F. Potential energy landscape of a coarse grained model for water: ML-BOP. *J. Chem. Phys.* **160**, 114502 (2024).
35. Adler, T., Knizia, G. & Werner, H. A simple and efficient CCSD(T)-F12 approximation. *J. Chem. Phys.* **127**, 221106 (2007).
36. Knizia, G., Adler, T. B. & Werner, H.-J. Simplified CCSD(T)-F12 methods: theory and benchmarks. *J. Chem. Phys.* **130**, 054104 (2009).
37. Stanton, J. F. Why CCSD(T) works: a different perspective. *Chem. Phys. Lett.* **281**, 130–134 (1997).

38. Rezac, J. & Hobza, P. Benchmark calculations of interaction energies in noncovalent complexes and their applications. *Chem. Rev.* **116**, 5038–5071 (2016).
39. Nesbet, R. Atomic Bethe-Goldstone equations. *Adv. Chem. Phys.* **14**, 1–34 (1969).
40. Hankins, D., Moskowitz, J. & Stillinger, F. Water molecule interactions. *J. Chem. Phys.* **53**, 4544–4554 (1970).
41. Paesani, F. Getting the right answers for the right reasons: toward predictive molecular simulations of water with many-body potential energy functions. *Acc. Chem. Res.* **49**, 1844–1851 (2016).
42. Babin, V., Leforestier, C. & Paesani, F. Development of a 'first principles' water potential with flexible monomers: dimer potential energy surface, VRT spectrum, and second virial coefficient. *J. Chem. Theory Comput.* **9**, 5395–5403 (2013).
43. Babin, V., Medders, G. R. & Paesani, F. Development of a 'first principles' water potential with flexible monomers. II: trimer potential energy surface, third virial coefficient, and small clusters. *J. Chem. Theory Comput.* **10**, 1599–1607 (2014).
44. Medders, G. R., Babin, V. & Paesani, F. Development of a 'first-principles' water potential with flexible monomers. III. Liquid phase properties. *J. Chem. Theory Comput.* **10**, 2906–2910 (2014).
45. Muniz, M. C. et al. Vapor-liquid equilibrium of water with the MB-pol many-body potential. *J. Chem. Phys.* **154**, 211103 (2021).
46. Bore, S. L. & Paesani, F. Realistic phase diagram of water from 'first principles' data-driven quantum simulations. *Nat. Commun.* **14**, 3349 (2023).
47. Reddy, S. K. et al. On the accuracy of the MB-pol many-body potential for water: interaction energies, vibrational frequencies, and classical thermodynamic and dynamical properties from clusters to liquid water and ice. *J. Chem. Phys.* **145**, 194504 (2016).
48. Palos, E. et al. Current status of the MB-pol data-driven many-body potential for predictive simulations of water across different phases. *J. Chem. Theory Comput.* **20**, 9269–9289 (2024).
49. Zhang, L., Han, J., Wang, H., Car, R. & E, W. Deep potential molecular dynamics: a scalable model with the accuracy of quantum mechanics. *Phys. Rev. Lett.* **120**, 143001 (2018).
50. Zhang, L. et al. End-to-end symmetry preserving inter-atomic potential energy model for finite and extended systems. *Adv. Neural Inf. Process. Syst.* **31**, 4436–4446 (2018).
51. Zhang, L., Lin, D.-Y., Wang, H., Car, R. & E, W. Active learning of uniformly accurate interatomic potentials for materials simulation. *Phys. Rev. Mater.* **3**, 023804 (2019).
52. Zhai, Y., Caruso, A., Bore, S. L., Luo, Z. & Paesani, F. A 'short blanket' dilemma for a state-of-the-art neural network potential for water: reproducing experimental properties or the physics of the underlying many-body interactions? *J. Chem. Phys.* **158**, 084111 (2023).
53. Muniz, M. C., Car, R. & Panagiotopoulos, A. Z. Neural network water model based on the MB-pol many-body potential. *J. Phys. Chem. B* **127**, 9165–9171 (2023).
54. Zhai, Y., Rashmi, R., Palos, E. & Paesani, F. Many-body interactions and deep neural network potentials for water. *J. Chem. Phys.* **160**, 144501 (2024).
55. Nguyen, A. H. & Molinero, V. Identification of clathrate hydrates, hexagonal ice, cubic ice, and liquid water in simulations: the CHILL+ algorithm. *J. Phys. Chem. B* **119**, 9369–9376 (2015).
56. Russo, J., Romano, F. & Tanaka, H. New metastable form of ice and its role in the homogeneous crystallization of water. *Nat. Mater.* **13**, 733–739 (2014).
57. Kumar, S., Rosenberg, J. M., Bouzida, D., Swendsen, R. H. & Kollman, P. A. The weighted histogram analysis method for free-energy calculations on biomolecules. I. The method. *J. Comp. Chem.* **13**, 1011–1021 (1992).
58. Bianco, V. & Franzese, G. Critical behavior of a water monolayer under hydrophobic confinement. *Sci. Rep.* **4**, 4440 (2014).
59. Sciortino, F., Gartner, I., Thomas, E. & Debenedetti, P. G. Free-energy landscape and spinodals for the liquid-liquid transition of the TIP4P/2005 and TIP4P/Ice models of water. *J. Chem. Phys.* **160**, 104501 (2024).
60. Mishima, O. & Sumita, T. Equation of state of liquid water written by simple experimental polynomials and the liquid–liquid critical point. *J. Phys. Chem. B* **127**, 1414–1421 (2023).
61. Malek, S. M., Poole, P. H. & Saika-Voivod, I. Thermodynamic and structural anomalies of water nanodroplets. *Nat. Commun.* **9**, 2402 (2018).

Methods

MD simulations

Classical MD simulations with the DNN@MB-pol model[46] were carried out using LAMMPS[62] through the DeePMD-kit[63,64] plug-in. All details about the DNN@MB-pol model are discussed elsewhere[46]. Details about the DeePMD-kit software package, including how DeePMD-based models handle the computation of energies, forces and virial are reported in other work[63,64]. All simulations were carried out under periodic boundary conditions for a system containing $N = 256$ water molecules. The initial configurations at each temperature were taken from the MB-pol simulations at 1 atm (ref. 65). The subsequent MD simulations were performed in the *NPT* ensemble. The temperature was maintained using a global Nosé–Hoover thermostat chain of length 3 with a relaxation time of 0.05 ps, and the pressure was controlled by a global Nosé–Hoover barostat with a relaxation time of 0.5 ps, which was thermostatted by a Nosé–Hoover thermostat chain of length 3. The MD trajectories were propagated with a time step of 0.5 fs using the velocity Verlet algorithm[66].

Density of states

To maximize the information contained in the extensive set of *NPT* simulations carried out with the DNN@MB-pol potential, $\Omega(V, E)$ was calculated via the weighted histogram analysis procedures[57], extended to the *NPT* ensemble[58] (Supplementary Section 3). From $\Omega(V, E)$, the probability $\mathcal{P}(V, E)$ of observing a thermodynamic state point, characterized by volume V and energy E at any given temperature T and pressure P (whether within the range covered by actual *NPT* simulations or extrapolated beyond it), can be calculated as

$$\mathcal{P}(V,E) = \frac{\Omega(V,E)\mathrm{e}^{-\beta(E+PV)}}{\sum_V\sum_E \Omega(V,E)\mathrm{e}^{-\beta(E+PV)}}. \quad (1)$$

Here $\beta = 1/k_\mathrm{B}T$ and

$$\mathcal{P}(V) = \sum_E \mathcal{P}(V,E), \quad \mathcal{P}(E) = \sum_V \mathcal{P}(V,E). \quad (2)$$

The average value of $\mathcal{P}(V)$ at fixed T and P, namely, $\langle V\rangle(P, T)$, provides the equation of state for the system of $N = 256$ water molecules simulated in this study. The logarithm of $\mathcal{P}(V)$ provides—except for a constant—the (restricted) Gibbs free energy βG at a given thermodynamic state point with temperature T and pressure P.

All the thermodynamic quantities can then be calculated from $\mathcal{P}(V, E)$. For example, the LDL–HDL coexistence line (Fig. 3) was determined by identifying the pressure at each temperature T, where $-k_\mathrm{B}T\ln[\mathcal{P}(V)]$ displays two minima of equal depth. Similarly, the LDL and HDL spinodal pressures can be calculated by identifying, for each temperature T, the pressure values at which the LDL and HDL minima disappear, respectively.

Data availability

All data used in the figures are available via GitHub (https://github.com/paesanilab/Data_Repository/tree/main/MB-pol_critical_point)[69]. The DNN@MB-pol potential used in the MD simulations, along with the corresponding training set, is publicly available via Zenodo (https://doi.org/10.5281/zenodo.7863744)[67]. The MB-pol potential used in the MD simulations is available in the MBX software[68,69]. Owing to their large sizes, all DNN@MB-pol and MB-pol MD trajectories are stored on a dedicated local server and are available from the corresponding author upon request.

Code availability

All DNN@MB-pol MD simulations were carried out with LAMMPS[62] patched with the DeePMD-kit plug-in[63]. All MB-pol simulations were carried out with LAMMPS[62] patched with the MBX software[68,69].

References

62. Thompson, A. P. et al. LAMMPS—a flexible simulation tool for particle-based materials modeling at the atomic, meso, and continuum scales. *Comput. Phys. Commun.* **271**, 108171 (2022).
63. Wang, H., Zhang, L., Han, J. & Weinan, E. DeePMD-kit: a deep learning package for many-body potential energy representation and molecular dynamics. *Comput. Phys. Commun.* **228**, 178–184 (2018).
64. Zeng, J. et al. DeePMD-kit v2: a software package for deep potential models. *J. Chem. Phys.* **159**, 054801 (2023).
65. Gartner III, T. E. et al. Anomalies and local structure of liquid water from boiling to the supercooled regime as predicted by the many-body MB-pol model. *J. Phys. Chem. Lett.* **13**, 3652–3658 (2022).
66. Shinoda, W., Shiga, M. & Mikami, M. Rapid estimation of elastic constants by molecular dynamics simulation under constant stress. *Phys. Rev. B* **69**, 134103 (2004).
67. Bore, S. & Paesani, F. Realistic phase diagram of water from 'first principles' data-driven quantum simulations. *Zenodo* https://doi.org/10.5281/zenodo.7863744 (2023).
68. Riera, M. et al. MBX: a many-body energy and force calculator for data-driven many-body simulations. *J. Chem. Phys.* **159**, 054802 (2023).
69. Paesani Lab. MBX: a many-body energy and force calculator. *GitHub* https://github.com/paesanilab/MBX (2019).

Acknowledgements

This research was supported by the Air Force Office of Scientific Research grant no. FA9550-20-1-0351 (Y.Z., S.L.B. and F.P.). F.S. acknowledges support from MIUR-PRIN grant no. 2022JWAF7Y, Cineca ISCRA initiative and ICSC-Centro Nazionale di Ricerca in High Performance Computing, Big Data and Quantum Computing, funded by the European Union ('NextGenerationEU'). Computational resources were provided by the Department of Defense High Performance Computing Modernization Program (HPCMP); the Advanced Cyberinfrastructure Coordination Ecosystem: Services & Support (ACCESS) program, which is supported by National Science Foundation grant nos. 2138259, 2138286, 2138307, 2137603 and 2138296; the Triton Shared Computing Cluster (TSCC) at the San Diego Supercomputer Center (SDSC); and the Scientific Computing Core at the Flatiron Institute, a division of the Simons Foundation.

Author contributions

F.S. and F.P. conceived and designed the research. Y.Z., S.L.B. and F.P. performed the simulations. F.S. and F.P. analysed the results and wrote the paper. F.S. and F.P. acquired funding. F.P. administered the project.

Competing interests

The authors declare no competing interests.

Additional information

Supplementary information The online version contains supplementary material available at https://doi.org/10.1038/s41567-024-02761-0.

Correspondence and requests for materials should be addressed to F. Paesani.

Peer review information *Nature Physics* thanks Roberto Car and the other, anonymous, reviewer(s) for their contribution to the peer review of this work.